Aeroelastic Characteristics of a Highly Flexible Aircraft

Marthinus C. van Schoor† and Andreas H. von Flotow*
Massachusetts Institute of Technology, Cambridge, Massachusetts

This paper describes an aeroelastic analysis performed on a human-powered aircraft. The structural characteristics of this aircraft (namely, very flexible wings, high aspect ratio, and low wing loadings) are typical of proposed high-altitude long-endurance aircraft. Because of these unique features, the aircraft exhibits uncommon aeroelastic characteristics. The structural dynamics of the airplane are obtained from a finite element model. In an assumed mode approach, a subset of the natural mode shapes is used to calculate the quasisteady and unsteady generalized modal forces using a two-dimensional strip model, which includes unsteady drag and leading-edge suction forces. The aeroelastic model predicts the airplane to be stable (at both sea level and high altitude), except for a mildly unstable phugoid mode. The results indicate that unsteady aerodynamics are significant for this type of aircraft and that the flexibility of the aircraft must be included to correctly model the dynamics for control purposes. A final conclusion is that the aircraft dynamics are highly dependent on the flight conditions (flight speed and altitude).

Nomenclature

A_i	= area of span station i
C_{D_0}	= parasite drag coefficient
C_{L_α}	= slope of lift curve
C_{M_0}	= aerodynamic moment about the aerodynamic center at zero angle of attack
b_i	= half chord ($c_i/2$) at span station i
d, D	= damping, damping matrix
e	= Oswald's efficiency factor
j	$=\sqrt{-1}$
m, M	= mass, mass matrix
k, K	= stiffness, stiffness matrix
q_∞	= freestream dynamic pressure = $(1/2)\,\rho U_\infty^2$
s_i	= width of aerodynamic strip i
U_i	= perturbed velocity in the x direction of the ith strip
U_∞	= freestream velocity
u,v,w	= X, Y and Z displacements/deformations, respectively
$\dot{u},\dot{v},\dot{w}$	= velocities in the X, Y and Z directions, respectively
ϕ,θ,ψ	= rotations about the X, Y and Z axes, respectively

Subscripts

d	= dynamic or perturbed
e	= equilibrium or steady state
i	= index to identify aerodynamic strip
u	= unsteady

Introduction

THE technology developed during MIT's *Daedalus* human-powered aircraft program is applicable to the development of high-altitude long-endurance aircraft (HALE). In order to stay aloft for extended periods of time, these aircraft[1] will need to be very light and aerodynamically efficient. Using on-board fuel, solar or microwave power for propulsion, HALE aircraft can be used as reconnaissance/communication vehicles or to gather high altitude scientific data. These types of aircraft are characterized by high aspect ratio wings, low wing loadings, very flexible structures, natural frequencies as low as 0.6 Hz, and air apparent mass as high as 35% of the total aircraft mass. A common assumption that aircraft rigid and flexible body dynamics can be separated cannot be applied to these aircraft. Separation of rigid body and structural dynamics is not justified nor is the approximation of quasisteady aerodynamics.

This paper describes the aeroelastic modeling and analysis of MIT's human-powered airplane, the *Michelob Light Eagle* (MLE). The MLE, shown in Fig. 1, extended the world distance record for human powered aircraft to 58 km in January 1987 and served as a prototype for the *Daedalus* aircraft, which extended the record to 130 km in the spring of 1988. The high aspect ratio and the Reynolds number at nominal flight speed of the MLE is comparable to those expected of high-altitude long-endurance aircraft. One might thus view the research reported in this paper as being prototypical of that required for the development of such high-altitude long-endurance aircraft. Table 1 summarizes the aerodynamic and structural properties of the MLE aircraft.

Zerweckh and von Flotow[2,3] outlined the attempted identification of the stability derivatives[4] of the MLE from flight-test data using a parameter identification program based upon assumed rigid body dynamics with quasisteady aerodynamics. Using these stability derivatives, the frequency of both the short period and phugoid mode was predicted to be within the range of the in-flight observed structural frequencies. This

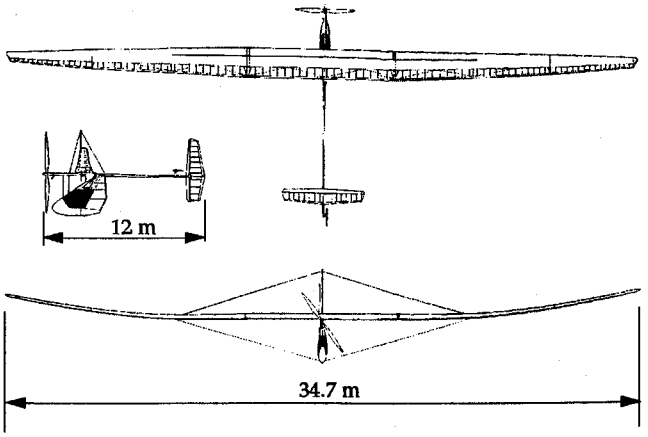

Fig. 1 The *Michelob Light Eagle* airplane.

Presented as Paper 89-1187 at the 30th AIAA Structural Dynamics and Materials Conference, Mobile, AL, April 3–5, 1989; received June 28, 1989; revision received May 2, 1990; accepted for publication June 4, 1990.

†Research Associate. Member AIAA.
*Assistant Professor. Member AIAA.

Table 1 MLE aerodynamic and structural properties

Aerodynamic and structural properties			
Wing Area	32.8 m^2	Drag Area	0.8 m^2
Wing Span	34.7 m	Aspect Ratio	36.7
Empty Weight	42.0 kg	Mass (With Pilot)	112.8 kg
Design Power	225.0 W	Airspeed	7.0 m/s
Wing Loading	34.0 N/m^2		

Moment of inertias			
Without apparent mass		With apparent mass	
I_x	2002 kgm^2	I_x	3920 kgm^2
I_y	205 kgm^2	I_y	340 kgm^2
I_z	2086 kgm^2	I_z	2910 kgm^2

Table 2 Summary of structural dynamic characteristics of the MLE[a]

Mode number	Frequency, Hz	Description
1	0.0	rigid body X translation
2	0.0	rigid body Y translation
3	0.0	rigid body Z translation
4	0.0	rigid body rotation about X axis
5	0.0	rigid body rotation about Y axis
6	0.0	rigid body rotation about Z axis
7	0.559	symmetric wing bending
8	0.677	tailboom rotation
9	0.879	1st asymmetric wing bending
10	1.134	1st symmetric wing bending (fore-aft)
11	1.183	1st tailboom bending (X-Y plane)
12	2.267	1st tailboom bending (X-Z plane)
13	2.336	2nd symmetric wing bending
14	2.603	2nd asymmetric wing bending
15	2.919	1st wing asymmetric torsion
16	4.147	3rd wing symmetric bending

[a]Calculated with sea level apparent mass added to the structural mass.

result reinforced engineering judgment that aeroelastic effects cannot be ignored in modeling the stability and control characteristics of the MLE. The research reported in this paper thus includes the aeroelastic and unsteady aerodynamic effects in the stability model in order to not only improve the analytical stability and control predictions but also to investigate the importance of these effects.

Aeroelastic Model

An aeroelastic model requires both a structural dynamic model and an aerodynamic model of the MLE. The next sections describe how these models are obtained.

Structural Dynamic Model

The structural dynamic model required for the aeroelastic analysis is obtained by modeling the MLE primary structure with finite elements. Beam finite elements are used. The structural properties for the beam elements are obtained from the original static airframe design. As an example, the wing is modeled with eight finite beam elements. The beam properties (namely, EI, GJ, and EA) mass and inertia are obtained by using their averages over the beam element's length. The mass of the ribs and the air contained inside the wing are split and lumped at the two beam nodes. Note that the air contained inside the wing is roughly 16% of the total wing mass.

The only modification to the finite element model was the adjustment of the EI values, so that the static deflections predicted by the finite element model matched the in-flight observed deflections of the wing at the lift-wire attachment points and at the wing tips. This was achieved by loading the finite element model of the aircraft with the steady aerodynamic loads and comparing the analytical deflections with the in-flight observed deflections. The modified EI values were within 15% of the original values.

Given the low natural frequencies of the MLE, a ground-vibration test will require a very flexible suspension system. In general, one order of magnitude separation between the support-systems natural frequency and the first natural frequency of the aircraft is required for reliable modal test results. The lowest suspension frequencies achieved by state-of-the-art suspension systems are 0.1 Hz, too high for testing the MLE. Thus, although modal test results would have greatly enhanced the validity of the results, budget and technology constraints require the presented results to be considered a preliminary study.

A standard finite element program was used to determine the structural dynamic characteristics of the MLE. The results are depicted in Fig. 2 and summarized in Table 2. In obtaining the results shown in Fig. 2, the apparent mass was added to the structural mass of the aircraft. At sea level, the aerodynamic apparent mass is approximately 35% of the total aircraft's mass. This mass was added to obtain the best possible set of assumed modes for the aeroelastic stability analysis. However, since the apparent mass is also included in the aerodynamic forces, the apparent mass was removed from the generalized structural mass matrix resulting in a nondiagonal modal mass matrix.

Pure rigid body modes (translation or rotation about one of the structural reference axes) were generated to enable the separation of longitudinal and lateral dynamics. The rigid body mode shapes generated by the finite element code are linear combinations of these motions.

Aerodynamic Model

The unsteady aerodynamic forces could have been obtained using a standard kernel function[5] or doublet lattice program. This approach was not taken for several reasons. A unique feature of the MLE structure is the very low stiffness of the main wing in the fore-aft direction. The first wing fore-aft symmetric bending mode falls between the first and second vertical wing bending modes. In addition, since the MLE's angle of attack at nominal flight speed is as high as 10 deg, it was felt that unsteady drag terms should be included in the aerodynamic model.[6,7] Therefore, to consistently and correctly include all terms, the unsteady aerodynamics are calculated using a two-dimensional strip model of the MLE (Fig. 3). It must be noted that this two-dimensional strip approach may yield conservative flutter speed predictions.[8]

For the aerodynamic model, the MLE's aerodynamic surfaces are divided into a finite number of two-dimensional strips. The aerodynamic lift and drag forces, as well as the aerodynamic moment, are calculated at the center of each of these aerodynamic strips. Although the forces are normally calculated at the 1/4- or 3/4-chord point, the force and moment expressions are significantly simplified by using the center of the aerodynamic strip.

The aerodynamic forces (and moments) are a combination of the steady, quasisteady, and unsteady lift, drag, and moments acting on the strip. The aerodynamic model assumes 1) that wing thickness effects can be ignored, 2) incompressible flow, 3) that chordwise deformations can be ignored, and 4) that the effect of one aerodynamic surface on another (for example, the wing on the elevator) can also be ignored. Given the relatively small size of the other aerodynamic surfaces (namely, the elevator, rudder, and cockpit) compared to the wing, this simplification is justified. The model divides the aerodynamic surfaces—the main wing, elevator, rudder, and cockpit—into a number of aerodynamic strips. The cockpit is included in the aerodynamic model to correctly model the lateral dynamics since the size of the cockpit is comparable to the rudder. The contributions of the lift, drag, and moment forces on a strip (i) can be transformed to yield the forces in the inertial reference frame (see Fig. 4). For example, the

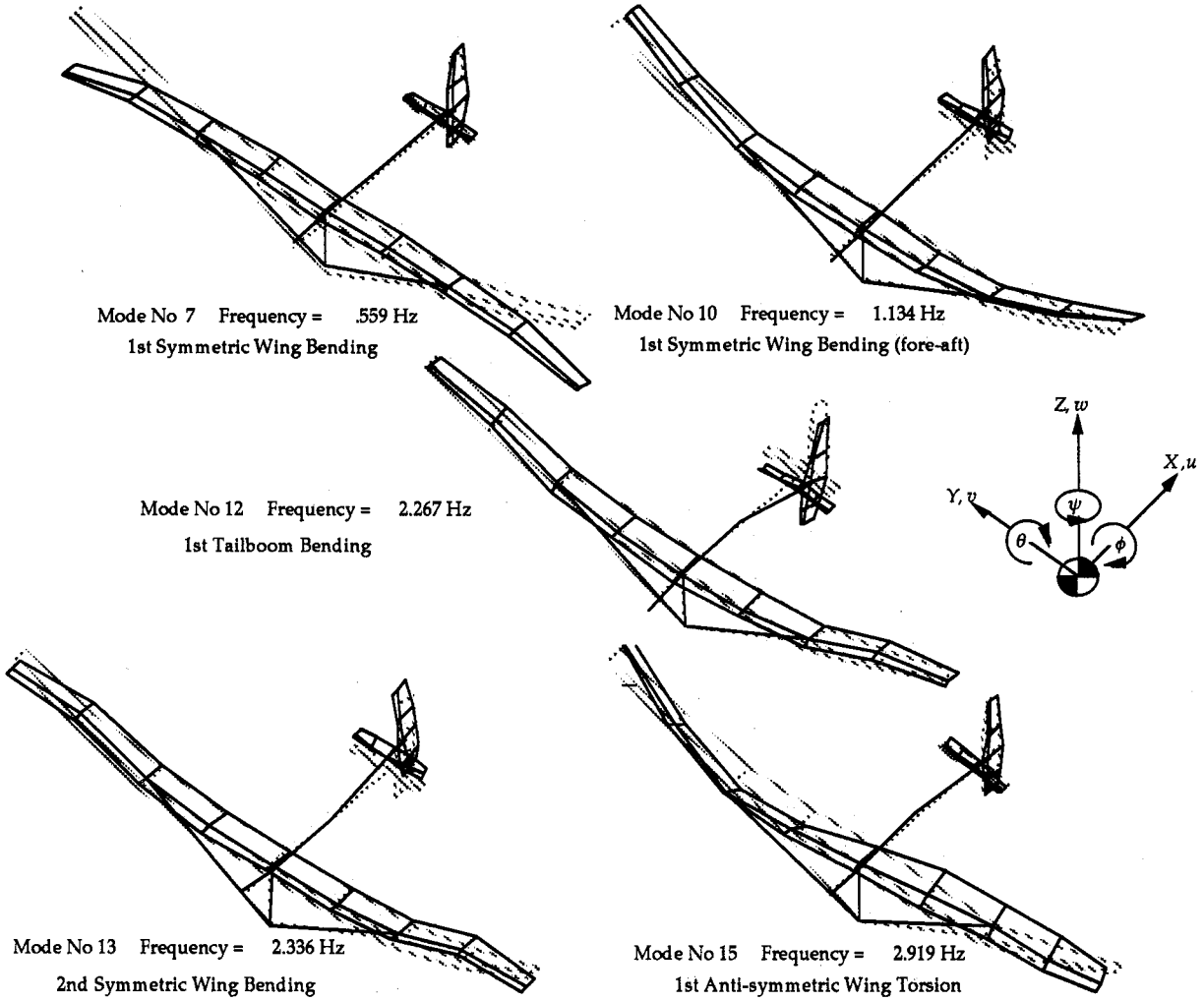

Fig. 2 Selected mode shapes of the MLE.

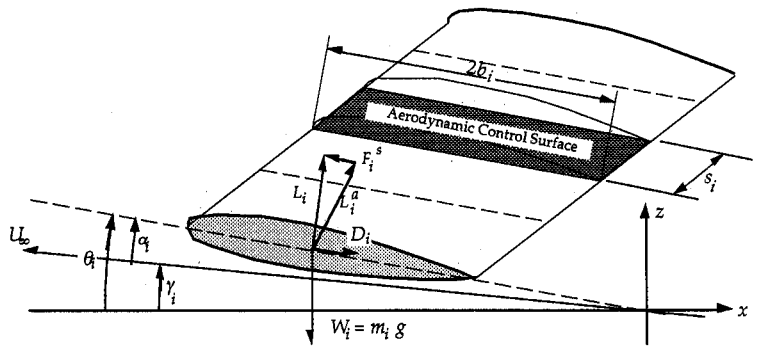

Fig. 3 Two-dimensional aerodynamic strip model with aerodynamic surface and sign convention.

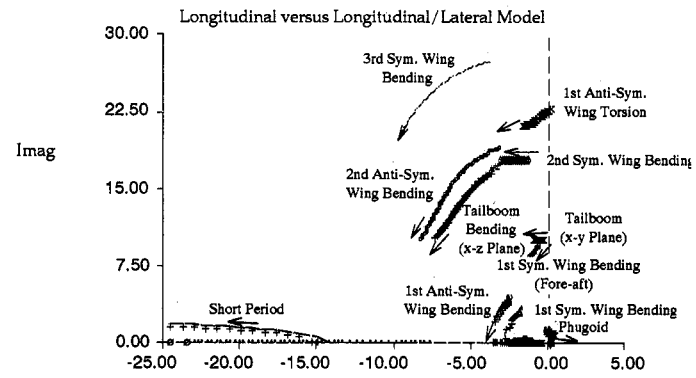

Fig. 4 Root loci of the MLE flying at sea level (6–22 m/s) for a 14 mode six-deg-of-freedom model and a truncated 8 mode longitudinal model.

force in the x direction:

$$F_i^x = +L_i^a \sin\theta_i + D_i \cos\gamma_i - F_i^s \cos\theta_i \tag{1}$$

the force in the z direction:

$$F_i^z = +L_i^a \cos\theta_i - D_i \sin\gamma_i + F_i^s \sin\theta_i - W_i \tag{2}$$

the pitching moment (y axis) about the half chord point:

$$M_i^y = M_{i_0}^y + (b_i/2)L_i^a \tag{3}$$

F_i^s is the unsteady leading-edge suction force that arises from the inverse square root singularity of the vorticity distribution along the airfoil at its leading edge. This propulsive force corrects for the freestream component of the lift, which is computed normal to the airfoil and thus yields a lift vector normal to the freestream.[6,9,10] Considering small perturbations about straight and level flight, the following small angle approximations can be made to linearize the equations of motion:

$$\gamma^i = \gamma_i^e (=0) + (\dot{w}_i/U_\infty) = \dot{w}_i/U_\infty \tag{4}$$

$$\theta_i = \theta_i + \theta_i^e \tag{5}$$

The streamwise velocity at the half chord of the section is perturbed as

$$U_i = U_\infty - \dot{u}_i \tag{6}$$

Using these approximations, Eqs. (1–3), for small angles, become

$$F_i^x = L_i^a(\theta_i^e + \theta_i) + D_i - F_i^s \tag{7}$$

$$F_i^z = L_i^a - D_i(\dot{w}_i/U_\infty) + F_i^s(\theta_i^e + \theta_i) - W_i \tag{8}$$

$$M_i^y = M_{i_0}^y + (b_i/2)L_i^a \tag{9}$$

The total lift is a combination of the steady and dynamic lift (Dowell[11])

$$L_i^a = (1/2)\,\rho(U_\infty - \dot{u}_i)A_i\{(U_\infty - \dot{u}_i)C_{L_\alpha}^i\theta_i^e + \pi b_i\dot{\theta}_i - C_{L_\alpha}^i C(k_i)[\dot{w}_i - (U_\infty - \dot{u}_i)\theta - (1/2)b_i\dot{\theta}_i]\} - (1/2)\rho A_i b_i \pi \ddot{w}_i \tag{10}$$

where $C(k_i)$ is the well-known Theodorsen function.[12] Given the high in-flight observed modal damping ratios, in this research, unlike common practice, the reduced frequency is considered to be complex. The expression for the generalized Theodorsen function[13,14] is

$$C(k_r) = \frac{K_1(k_r)}{K_0(k_r) + K_1(k_r)} \tag{11}$$

The functions K_i are modified Bessel functions and k_r is the complex reduced frequency. Note that Jone's approximation for the generalized Theodorsen function could also have been used with little loss in accuracy. The drag on the aerodynamic strip is

$$D_i = (1/2)\rho(U_\infty - \dot{u}_i)^2 A_i(C_{D_0} + C_{D_{\text{induced}}}^i) \tag{12}$$

and the leading-edge suction force is obtained from Boyd[6] as

$$F_i^s = C_{L_\alpha}^i \rho(U_\infty - \dot{u}_i)A_i\{-C(k_i)\dot{w}_i + (U_\infty - \dot{u}_i)C(k_i)\theta_i + [(1/2)C(k_i) - (1/2)]b_i\dot{\theta}_i\}\theta_i^e \tag{13}$$

In the model, the spanwise lift distribution is modified and induced drag is included to account for some of the three-dimensional aerodynamic effects. The spanwise lift distribution is assumed to be elliptical

$$C_{L_\alpha}^i = 2\pi C_0\sqrt{1 - (y_i/y_{\text{tip}})^2} \tag{14}$$

where C_0 is constant for a given aerodynamic surface (wing, elevator, etc.) and determined to yield the correct steady total lift. The expression used for the sectional induced drag[15] is

$$C_{D_{\text{induced}}}^i = \frac{C_{L_\alpha}^{i2}[\theta_i^e + \theta_i - (\dot{w}_i/U_\infty)]^2}{\pi e A} \tag{15}$$

Although this term is zero for wings of infinite span, the high steady-state angle of attack of 10 deg at nominal flight speed makes this term as important as the parasitic drag term. The moment about the center of the aerodynamic strip (midchord) is given by Dowell[11] as

$$M_i^y = (1/2)\rho(U_\infty - \dot{u}_i)^2 A_i b_i[C_{M_0}^i + (1/2)C_{L_\alpha}^i\theta_i^e] + (1/2)\pi\rho A_i b_i[-1/2(U_\infty - \dot{u}_i)b_i\dot{\theta}_i - (1/8)b_i^2\ddot{\theta}_i] + (1/4)\rho(U_\infty - \dot{u}_i)A_i b_i C(k_i) \times C_{L_\alpha}^i[-\dot{w}_i + (U_\infty - \dot{u}_i)\theta_i + (1/2)b_i\dot{\theta}_i] \tag{16}$$

The perturbational force (or moment) due to perturbations q_i (u_i, v_i, w_i, ψ_i, and θ_i) is obtained by linearizing about the equilibrium state, namely, level flight

$$\delta F_j = \frac{\partial F_j}{\partial q_1}q_1 + \frac{\partial F_j}{\partial q_2}q_2 + \frac{\partial F_j}{\partial q_3}q_3 + \cdots \tag{17}$$

The governing differential equations are obtained by evaluating the partial derivatives of Eq. (17). Setting all second-order terms to zero and assuming complex quasiperiodic motion

$$u(x,y,z,t) = \boldsymbol{u}(x,y,z)e^{\lambda t}$$
$$v(x,y,z,t) = \boldsymbol{v}(x,y,z)e^{\lambda t}$$
$$w(x,y,z,t) = \boldsymbol{w}(x,y,z)e^{\lambda t} \tag{18}$$

Let

$$k_i = k_r b_i/b_r, \quad \lambda = j(k_r U_\infty/b_r) \quad \text{and} \quad \lambda_2 = -(k_r U_\infty/b_r)^2 \tag{19}$$

where b_r is a reference length taken to be the half chord length at the 70% span position. The aerodynamic perturbational forces and moment acting on the aerodynamic strip are given by

$$\frac{\delta F_i^x}{q_\infty A_i e^{\lambda t}} = -2C_{D_0}\left(\frac{\lambda}{U_\infty}\right)u_i + \pi b_i\left(\frac{\lambda}{U_\infty}\right)\theta_i^e\theta_i - \pi b_i\left(\frac{\lambda}{U_\infty}\right)^2\theta_i^e w_i + \left\{\left[1 - 2\frac{C_{L_\alpha}^{i2}}{\pi e A}\right]\left(\frac{\lambda}{U_\infty}\right) + \left(\frac{jk_r}{b_r}\right)[C(k_i) - 1]\right\}C_{L_\alpha}^i\theta_i^e w_i + \frac{1}{2}\left\{4\frac{C_{L_\alpha}^i}{\pi e A} + b_i\left(\frac{\lambda}{U_\infty}\right) - [C(k_i) - 1]\left[2 + \left(\frac{jk_r}{b_r}\right)b_i\right]\right\}C_{L_\alpha}^i\theta_i^e\theta_i \tag{20}$$

$$\frac{\delta F_i^z}{q_\infty A_i e^{\lambda t}} = -2\left(\frac{\lambda}{U_\infty}\right)C_{L_\alpha}^i\theta_i^e u_i + \pi b_i\left(\frac{\lambda}{U_\infty}\right)\theta_i - \left[(C_{L_\alpha}^i + C_{D_0})\left(\frac{\lambda}{U_\infty}\right) + \pi b_i\left(\frac{\lambda}{U_\infty}\right)^2\right]w_i - \left(\frac{jk_r}{b_r}\right)[C(k_i) - 1]C_{L_\alpha}^i w_i + \left\{1 + \frac{1}{2}b_i\left(\frac{\lambda}{U_\infty}\right) + [C(k_i) - 1]\left[1 + \frac{1}{2}\left(\frac{jk_r}{b_r}\right)b_i\right]\right\}C_{L_\alpha}^i\theta_i \tag{21}$$

$$\frac{\delta M_i^y}{q_\infty A_i b_i e^{\lambda t}} = +2C_{M_0}^i\left(\frac{\lambda}{U_\infty}\right)u_i - C_{L_\alpha}^i\left(\frac{\lambda}{U_\infty}\right)\theta_i^e u_i$$
$$-\left[\frac{1}{2}\pi b_i\left(\frac{\lambda}{U_\infty}\right)+\frac{1}{8}\pi b_i^2\left(\frac{\lambda}{U_\infty}\right)^2\right]\theta_i$$
$$-\left\{\frac{1}{2}\left(\frac{\lambda}{U_\infty}\right)+\left(\frac{jk_r}{b_r}\right)\frac{1}{2}[C(k_i)-1]\right\}C_{L_\alpha}^i w_i$$
$$+\left\{\frac{1}{2}-\frac{1}{4}b_i\left(\frac{\lambda}{U_\infty}\right)+\frac{1}{2}[C(k_i)-1]\left[1+\frac{1}{2}\left(\frac{jk_r}{b_r}\right)b_i\right]\right\}C_{L_\alpha}^i\theta_i \tag{22}$$

In these equations, terms containing the steady-state angle of attack (θ_e) are dependent on the equilibrium angle of attack and thus on flight speed. For the vertical surfaces, the equilibrium angle of attack is zero and the aerodynamic forces and moment acting on the aerodynamic strips are

$$\frac{\delta F_i^x}{q_\infty A_i e^{\lambda t}} = -2C_{D_0}\left(\frac{\lambda}{U_\infty}\right)u_i \tag{23}$$

$$\frac{\delta F_i^y}{q_\infty A_i e^{\lambda t}} = \pi b_i\left(\frac{\lambda}{U_\infty}\right)\psi_i$$
$$-\left\{[C_{L_\alpha}^i + C_{D_0}]\left(\frac{\lambda}{U_\infty}\right)+\pi b_i\left(\frac{\lambda}{U_\infty}\right)^2\right\}v_i$$
$$-\left(\frac{jk_r}{b_r}\right)[C(k_i)-1]C_{L_\alpha}^i v_i$$
$$+\left\{1+\frac{1}{2}b_i\left(\frac{\lambda}{U_\infty}\right)+[C(k_i)-1]\left[1+\frac{1}{2}\left(\frac{jk_r}{b_r}\right)b_i\right]\right\}C_{L_\alpha}^i\psi_i \tag{24}$$

$$\frac{\delta M_i^z}{q_\infty A_i b_i e^{\lambda t}} = +2C_{M_0}^i\left(\frac{\lambda}{U_\infty}\right)u_i$$
$$-\left[\frac{1}{2}\pi b_i\left(\frac{\lambda}{U_\infty}\right)+\frac{1}{8}\pi b_i^2\left(\frac{\lambda}{U_\infty}\right)^2\right]\psi_i$$
$$-\left\{\frac{1}{2}\left(\frac{\lambda}{U_\infty}\right)+\left(\frac{jk_r}{b_r}\right)\frac{1}{2}[C(k_i)-1]\right\}C_{L_\alpha}^i v_i$$
$$+\left\{\frac{1}{2}-\frac{1}{4}b_i\left(\frac{\lambda}{U_\infty}\right)+\frac{1}{2}[C(k_i)-1]\left[1+\frac{1}{2}\left(\frac{jk_r}{b_r}\right)b_i\right]\right\}C_{L_\alpha}^i\psi_i \tag{25}$$

The terms containing (λ) are included in the equations of motion as mass, damping, and stiffness terms. The $[C(k)-1]$ terms are calculated for a range of reference complex reduced frequencies $k_r = \rho_r e^{i\theta_r}$. The range of magnitudes and phase angles of the reference reduced frequency is selected to cover the range of reduced frequencies expected in the stability analysis. For quasisteady aerodynamics, the reduced frequency $k = 0$, and since $C(k=0) = 1$, a quasisteady aerodynamic model can be obtained by setting these terms equal to zero.

In an assumed mode approach, the deflections are represented as a linear superposition

$$u(x_i,y_i,z_i,t) = \sum_{n=1}^{m}\phi_n^x(x_i,y_i,z_i)q_n(t)$$
$$v(x_i,y_i,z_i,t) = \sum_{n=1}^{m}\phi_n^y(x_i,y_i,z_i)q_n(t)$$
$$w(x_i,y_i,z_i,t) = \sum_{n=1}^{m}\phi_n^z(x_i,y_i,z_i)q_n(t) \tag{26}$$

with the slopes given by

$$\psi(x_i,y_i,z_i,t) = \sum_{n=1}^{m}\frac{d\phi_n^y(x_i,y_i,z_i)}{dx}q_n(t)$$
$$\theta(x_i,y_i,z_i,t) = \sum_{n=1}^{m}\frac{d\phi_n^z(x_i,y_i,z_i)}{dx}q_n(t) \tag{27}$$

Using these expressions, the generalized aerodynamic force vector is given by

$$\boldsymbol{Q} = \phi^{xT}\delta\boldsymbol{F}^x + \phi^{yT}\delta\boldsymbol{F}^y + \frac{d\phi^{yT}}{dx}\delta\boldsymbol{M}^x + \phi^{zT}\delta\boldsymbol{F}^z + \frac{d\phi^{zT}}{dx}\delta\boldsymbol{M}^y \tag{28}$$

where the aerodynamic vectors $\boldsymbol{F}$ and $\boldsymbol{M}$ are defined by Eqs. (20–25).

Aeroelastic Differential Equations

The MLE was divided into four structural surfaces (namely, wing, elevator, rudder, and cockpit), and for each surface, a separate two-dimensional spline was fitted to the mode shapes obtained from the structural dynamic model. The airplane was also divided into several aerodynamic strips, and the deflection and rotation of the strip, required to calculate the aerodynamic loads on the strip [Eqs. (20–25)], could be evaluated using these fitted splines.

The aeroelastic governing differential equations are

$$[\boldsymbol{M}(\rho)\lambda^2 + \boldsymbol{D}(\rho,U_\infty,\theta_e)\lambda + \boldsymbol{K}(\rho,U_\infty,\theta_e)$$
$$-\boldsymbol{Q}_{ua}(\rho,U_\infty,\theta_e,\lambda)]e^{\lambda t} = 0 \tag{29}$$

The quasisteady aerodynamics are included in $\boldsymbol{M}$, $\boldsymbol{D}$, and $\boldsymbol{K}$, whereas $\boldsymbol{Q}_{ua}$ contains only the unsteady-aerodynamic terms. In the analysis, mass proportional damping is used. The damping ratio assumed for all the flexible modes is 2% ($\zeta = 0.02$).

Stability Analysis

In the stability analysis program, the steady-state angle of attack (θ_e) is calculated for each flight speed and altitude (air density). It is assumed that this angle is constant for a given aerodynamic surface (wing, elevator, etc.). Given the steady-state angle of attack, the corresponding terms in the generalized force matrices [Eq. (29)] are evaluated.

The aeroelastic stability characteristics are obtained by finding the eigenvalues of the characteristic equation. This is achieved using Mueller's method[16] to solve for the eigenvalues by finding the complex roots of the determinant of the characteristic equation [Eq. (29)]. Mueller's method is an iterative Newton-Raphson scheme that converges rapidly on the roots, given a good initial guess. At any given iteration, the reduced frequency [Eq. (19)] associated with the estimated root is calculated, and the corresponding unsteady generalized force matrix is obtained by linear two-dimensional interpolation in the reduced frequency magnitude and phase plane. The error introduced by the interpolation for the generalized force matrix is minimized by careful selection of the range of reduced frequency magnitude and phase values for which these matrices are calculated. The convergence in finding the roots is significantly slowed (double the computing time) by adding the unsteady aerodynamic terms.

The results of the aeroelastic stability analysis are presented in the form of root loci, where the solution (eigenvalues) at each flight speed is plotted on the real/imaginary plane. A root locus is only valid for the given altitude (air density).

Results

The aeroelastic stability results for the MLE flying at sea level, using the aeroelastic model described in previous sections, are depicted in Fig. 4. In the analysis, the first 14 modes of the MLE (Table 2) are used as well as the full unsteady

aerodynamic model. Also shown in this figure are the results of a truncated eight mode longitudinal model, which will be discussed in the next section. The root loci in Fig. 4 are obtained by increasing the airspeed from just below the MLE's stall speed (6 m/s) to 22 m/s, with speed increments of 0.25 m/s. The arrows in the figure indicate the direction of increasing flight speed.

The results show that the MLE is stable at this altitude except for the phugoid mode, which experienced a mild instability. The short period mode changes from a critically damped mode at low flight speeds to a highly damped oscillatory mode at higher flight speeds. At the nominal flight speed (7 m/s), the model predicts the phugoid mode to have a frequency of 0.17 Hz and a damping ratio of 16% (of critical). The short period mode, at this flight speed, is critically damped at the time constant of approximately 16 s. These values agree favorably with the results reported by Zerweckh.[2] Zerweckh used a rigid body model[17] to identify the MLE's stability coefficients from flight-test data with a parameter identification algorithm. Although not shown on the figure, the model also predicts an unstable spiral mode and a stable Dutch roll mode.

The significant changes in damping ratios indicate that an aeroelastic model is required to reliably predict the fatigue characteristics of very flexible aircraft, such as the MLE, or to identify critical structural components.

Sensitivity Study

The aeroelastic model developed in this research can also be used to investigate several key questions associated with highly flexible aircraft. Not only can the model be used to identify the relative importance of the modeling terms added to the traditional aeroelastic model but the model can also be used to determine aeroelastic stability characteristics of these types of aircraft for control and performance purposes.

In identifying the relative importance of the modeling terms added to the aeroelastic model, the following questions are addressed: Given no clear spectral separation between structural modes, how can the model be truncated? Are the unsteady aerodynamic terms important? Is it necessary to add the drag terms?

Model Complexity Issues

Separation of Longitudinal and Lateral Dynamics

Given that the MLE is almost symmetric with respect to the X-Z plane, it is expected that a model that is truncated to include only longitudinal modes would yield results for the longitudinal motion very similar to those obtained with the six degree-of-freedom, 14 mode model used to obtain the results in Fig. 4. This prediction is confirmed when the root loci of an aeroelastic analysis using an eight mode longitudinal model is overplotted on the results of the 14 mode, six degree-of-freedom model (Fig. 4). The modes included in this longitudinal model are the three longitudinal rigid body modes and the first five symmetric flexible modes (modes 7, 10, 12, 13, and 16 of Table 2). Given that for most of the roots the loci are identical, it can be concluded that the longitudinal and lateral dynamics can be separated.

In order to simplify the interpretation of the sensitivity studies, the longitudinal model will be used to determine the relative importance of the modeling terms.

Model Truncation

The effects of model truncation can be studied by comparing the convergence of the stability results as the number of flexible modes included in the model are increased. Figure 5 depicts the stability results for a three degree-of-freedom rigid body longitudinal model overplotted on the results of the eight mode longitudinal model. In this figure, only the relevant modes of the eight mode model are shown. The figure clearly shows that the stability results are significantly altered by the inclusion of the flexible modes. The rigid body model predicts a stable phugoid mode, compared to the combined rigid/flexible model that predicts a phugoid mode in which stability is dependent on the airspeed.

Quasisteady vs Unsteady Aerodynamics

In order to determine the relative importance of the unsteady aerodynamic terms, the aeroelastic analysis is repeated with a quasisteady aerodynamic model. The quasisteady aerodynamic model is obtained by setting the $[C(k) - 1]$ [see Eq. (25)] equal to zero. The results, together with the results of the unsteady aerodynamic model (Fig. 4) are plotted in Fig. 6. Given the significant difference between the results obtained with the two aerodynamic models, the conclusion can be reached that the unsteady aerodynamic terms are significant and that they should be retained in the aeroelastic stability analysis of these types of aircraft.

Unsteady Aerodynamic Drag Terms

The importance of the unsteady drag terms is investigated by repeating the aeroelastic analysis (Fig. 4) with the unsteady aerodynamic drag terms set to zero. In Fig. 7, the results of this model without the drag terms are overplotted on the results of the model where the unsteady drag terms are included. The results of the two models are almost identical; for example, the difference between the loci of the first symmetric fore-aft mode, shown in the blown-up area, is small. The conclusion is that the unsteady drag terms do not result in significant modal coupling between vertical and fore-aft motions. However, it must be noted that the addition of the unsteady drag terms slightly increases the damping of the fore-aft bending modes.

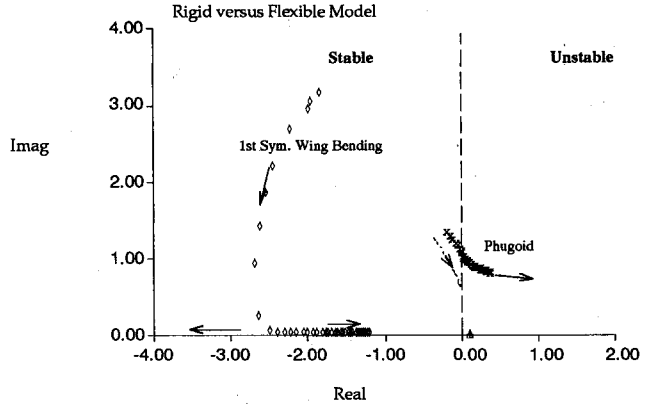

Fig. 5 Root loci comparison of the aeroelastic stability results for a flexible and rigid structural model.

(*Symbols* = 8 mode flexible model, *Lines* = Rigid structural model)

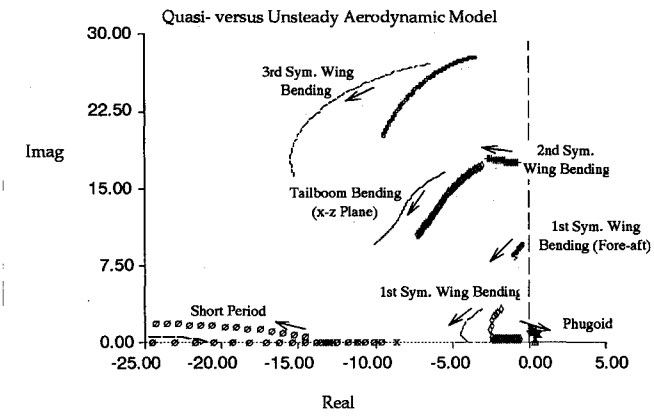

Fig. 6 Comparison of the root loci of two aeroelastic models. One model using unsteady and the other quasisteady aerodynamics. Results are for an eight mode longitudinal structural model for the MLE flying at sea level.

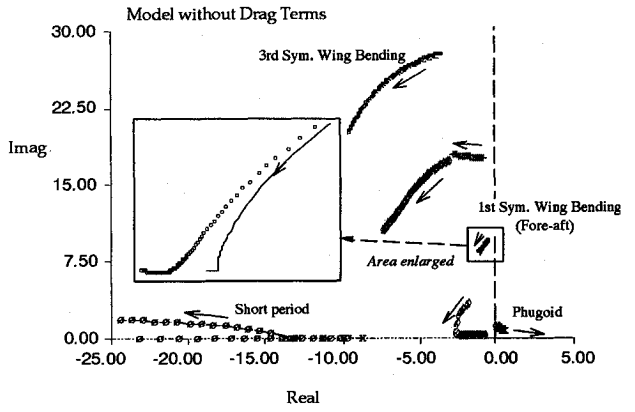

Fig. 7 Comparison of the root loci of two aeroelastic models. One model with and the other without unsteady aerodynamic drag terms. Results are for an eight mode longitudinal structural model of the MLE flying at sea level.

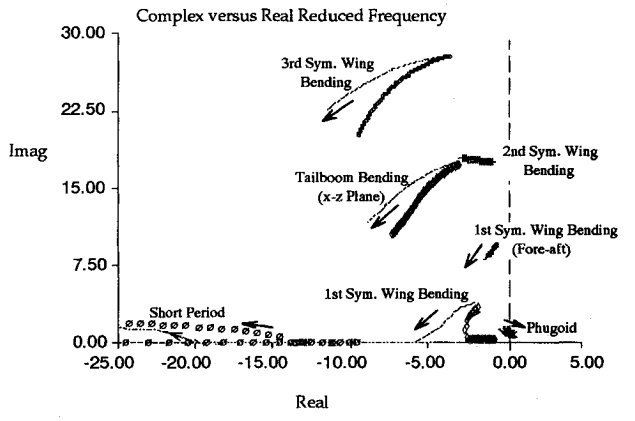

Fig. 8 Comparison of the root loci of two aeroelastic models. One model using real and the other complex reduced frequencies. Results are for an eight mode longitudinal structural model of the MLE flying at sea level.

Complex Reduced Frequency

The expression of the Theodorsen function as a complex function of the complex reduced frequency is justified by the relatively high damping ratios predicted by the aeroelastic model. If the reduced frequency is assumed to be real,[18] as is normally done in the aeroelastic analyses of lightly damped aircraft, the contribution due to the imaginary (damping) component of the reduced frequency would have been ignored. This would represent a significant mismodeling of the unsteady aerodynamics.

This conclusion is supported by results shown in Fig. 8. In this figure, the results of a model in which real reduced frequencies are used is compared with the results of the model based on complex reduced frequencies (Fig. 8). The difference between the root loci predicted by the two models is significant. In general, the model using real reduced frequencies predicts higher modal damping ratios than the model that uses complex reduced frequencies.

Control and Performance Issues

In order to determine the dependence of the eigenvalues on altitude, the aeroelastic analysis for the eight mode longitudinal model is repeated at the 20-km altitude. The 20-km altitude is a typical mission altitude proposed for HALE aircraft. The results are depicted in Fig. 9, in which the airspeed is varied from near stall (20 m/s) to 60 m/s in increments of 0.25 m/s.

It is important to notice the difference between the predictions for sea level (Fig. 4) and high altitude conditions (Fig. 9). At high altitudes, the mass ratio approaches zero and the

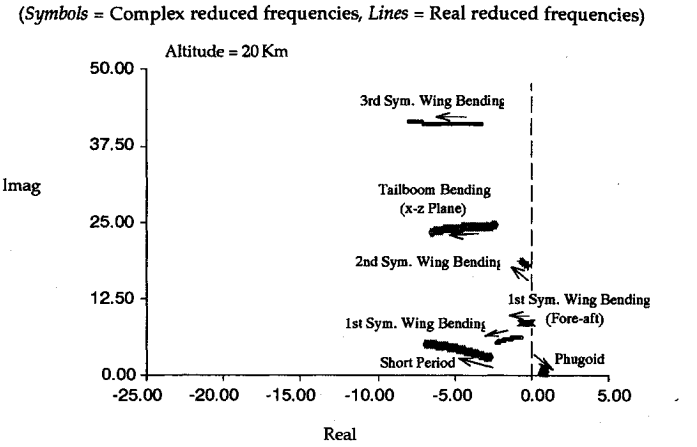

Fig. 9 Root loci of the MLE flying at 20-km altitude using unsteady aerodynamics and an eight mode longitudinal model.

modal frequencies are closer to the in-vacuo frequencies. The mass ratio is the air apparent mass divided by the structural mass. The resultant change in modal separation alters the aeroelastic modal coupling, and the overall conclusion is that any autopilot design will require static-pressure-dependent feedback gains for this wide range of model parameters. In conclusion, it is clear that aeroelastic effects cannot be ignored by a control engineer.

The phugoid mode, on which stability is dependent on the airspeed, is a low-frequency, very lightly unstable mode, which should be easy to control. At high altitudes, this mode is unstable for all flight speeds. Also interesting to note is that at low altitudes, the first wing bending mode changes from an oscillatory mode to a critically damped mode as the flight speed increases. This characteristic was verified by in-flight tests with the MLE. Note also that at low altitudes, the short period mode changes from a critically damped mode to an oscillatory mode as the flight speed increases.

From a structural engineering viewpoint, the significant changes in frequencies and damping ratios indicate that the aeroelastic model is a prerequisite for a reliable fatigue prediction.

Summary

This investigation identified the critical aeroelastic issues that should be considered in the aeroelastic analysis of very flexible, very light aircraft. Given the unverified structural dynamic model, the results can only be seen as preliminary, but the trends predicted should yield valuable insight to control and structural engineers. Specifically, the significant motion of the eigenvalues with airspeed and altitude indicates that an autopilot design, for these types of aircraft, will be a critical design activity.

The results indicate that simplification of the aeroelastic model by separation of rigid body modes and flexible modes is not justified and that many flexible modes may be required to yield a reliable aeroelastic model. In terms of modal coupling, the inclusion of unsteady aerodynamic drag terms is not required, but the damping, added to the fore-aft bending modes, introduced by these terms may alter the fatigue characteristics of the aircraft. The results also indicate that unsteady aerodynamic terms are important and that aeroelastic solution requires the use of complex reduced frequencies.

References

[1]Hall, D. W., Fortenbach, C. D., Dimicelli, B. V., and Parks, R. W., "A Preliminary Study of Solar Powered Aircraft and Associated Power Trains," NASA CR-3699, Dec. 1983.

[2]Zerweckh, S. H., Von Flotow, A. H., and Murray, J. E., "Flight Testing a Highly Flexible Aircraft; Case Study on the MIT Light Eagle," *Proceedings of the AIAA Atmospheric Flight Mechanics Conference*, AIAA, Washington, DC, Aug. 1988, pp. 405–414.

[3]Zerweckh, S. H., and Sullivan, R. B., "Results of the Flight Test Program with the Light Eagle and the Daedalus Aircraft," NASA Contractor Rep, NAG-1-836, Aug. 1988.

[4]Hill, K. W., "Estimation of Aerodynamic Characteristics from Dynamic Flight Test Data. Dynamic Stability Parameters," AGARD-CP-235, Paper 15, Nov. 1978.

[5]Cunningham, A. E., "A Collocation Method for Predicting Subsonic Pressure Distribution on Interfering Parallel Wings," *Proceedings of the 12th ASME Structures, Structural Dynamic and Materials Conference*, American Society of Mechanical Engineers, New York, 1971.

[6]Boyd, W. N., "Effect of Chordwise Forces and Deformations due to Steady Lift on Wing Flutter," Ph.D. Thesis, Stanford University, Stanford, CA, Dec. 1977.

[7]Petre, A., and Ashley, H., "Drag Effects on Wing Flutter," *Journal of Aircraft*, Vol. 13, No. 10, 1976, pp. 755–763.

[8]Rodden, W. P., "The Role of Structural and Aerodynamic Damping on the Aeroelastic Behavior of Wings," *Journal of Aircraft*, Vol. 25, No. 3, 1988, pp. 286–288.

[9]Garrick, I. E., "Propulsion of a Flapping and Oscillating Airfoil," NACA Rept. 567, May 1936.

[10]Greenberg, J. M., "Some Considerations on an Airfoil in an Oscillating Stream," NACA TN-1372, Aug. 1947.

[11]Dowell et al., *A Modern Course in Aeroelasticity*, Sijthoff and Noordhoff, Alpen aan den Rijn, the Netherlands, 1980.

[12]Bisplinghoff, R. L., Ashley, H., and Halfman, R. L., *Aeroelasticity*, Addison-Wesley, Cambridge, MA, Feb. 1955.

[13]Edwards, J. W., "Unsteady Aerodynamic Modeling and Active Aeroelastic Control," Dept. of Aeronautics and Astronautics, Stanford Univ., Stanford, CA, Rept. 504, Feb. 1977.

[14]Luke, Y. L., and Dengler, M. A., "Tables of the Theodorsen Circulation Function for Generalized Motion," *Journal of the Aeronautical Sciences*, Vol. 8, No. 7, 1951.

[15]McCormick, B. W., *Aerodynamics, Aeronautics, and Flight Mechanics*, Wiley, New York, 1979.

[16]Press, W. H., Flannery, B. P., TeuKolsky, S. A., and Vetterling, W. T., *Numerical Recipes—The Art of Scientific Computing*, Cambridge Univ., New York, 1987.

[17]Etkin, B., *Dynamics of Flight*, Wiley, New York, 1959.

[18]Hassig, H. J., "An Approximate True Damping Solution of the Flutter Equation by Determinant Iteration," *Journal of Aircraft*, Vol. 8, No. 11, 1971, pp. 885–889.